Journal of Photochemistry and Photobiology A: Chemistry 206 (2009) 10–17

Contents lists available at ScienceDirect

Journal of Photochemistry and Photobiology A: Chemistry

journal homepage: www.elsevier.com/locate/jphotochem

The complex photo-rearrangement of a heterocyclic N-oxide: Kinetics from picoseconds to minutes

Thorben Cordes[a,b], Nadja Regner[a], Björn Heinz[a], Elina Borysova[a], Gerald Ryseck[a], Peter Gilch[a,c,*]

[a] Lehrstuhl für BioMolekulare Optik, Fakultät für Physik, Ludwig-Maximilians-Universität, Oettingenstr. 67, D-80538 München, Germany
[b] Lehrstuhl für Angewandte Physik - Biophysik, Fakultät für Physik, Ludwig-Maximilians-Universität, Amalienstr. 54, D-80799 München, Germany
[c] Institut für Physikalische Chemie, Heinrich-Heine Universität Duesseldorf, 40225 Duesseldorf, Germany

ARTICLE INFO

Article history:
Received 27 February 2009
Received in revised form 4 May 2009
Accepted 7 May 2009
Available online 22 May 2009

Keywords:
Heteroaromatic N-oxides
Femtosecond spectroscopy
Fluorescence spectroscopy
UV/vis spectroscopy
IR spectroscopy

ABSTRACT

The photo-induced rearrangement of 2-benzoyl-3-phenylquinoxaline-1,4-dioxide yielding 1,3-dibenzoylbenzimidazolone (DBBI) is studied by time-resolved fluorescence, UV/vis absorption, and IR spectroscopy. This complex rearrangement occurs on time scales ranging from 0.1 ps up to minutes. Processes within the excited singlet state(s) (0.1–1 ps) are followed by a multi-phasic depletion of the fluorescent states (time constants of 1–200 ps). During that depletion both a triplet state and a precursor of the photo-product are populated. In absence of oxygen the triplet state decays in 8 μs. It does not participate in the formation of the photoproduct. A process with a time constant of 77 min terminates the product formation. It can be assigned to a hindered rotation of the benzoyl residues in DBBI.

1. Introduction

Imino N-oxides exhibit a rich and complex photochemistry [1,2]. Photo-excitation of imino N-oxides can, for instance, result in the formation of three-membered rings, ring expansions, ring cleavages or oxygen migrations [2]. The rearrangements often yield molecular motifs difficult to access otherwise rendering them of interest for the synthetic chemist. Further, the rearrangements — being photoreactions — can be studied by (highly) time-resolved spectroscopy. Such experiments yield kinetic data on the elementary reaction steps involved. The photochemistry of imino N-oxides could thus serve as an "instrument" for mechanistic organic chemistry.

A reaction (Scheme 1) which highlights the complexity of the N-oxide photochemistry is the rearrangement of 2-benzoyl-3-phenylquinoxaline-1,4-dioxide ($BPQO_2$) yielding 1,3-dibenzoylbenzimidazolone (DBBI) [3,4]. In the course of the reaction, the six-membered pyrazine ring of the quinoxaline scaffold transforms into a five-membered imidazolone ring — the molecule loses its N-oxide functional groups and forms two additional carbonyl groups. Such a large scale rearrangement suggests that various elementary steps have to occur during this reaction. Apart from steady state results reported by Masoud and Olmsted [4] there are no data on the kinetics of this reaction. In general, time-resolved data on the photochemistry of N-oxides are scarce. Those relevant for the present study will be presented in Section 4. The central findings of Masoud and Olmsted [4] are summarized as follows. They determined the quantum yield ϕ_p of the DBBI formation (Scheme 1) to be ~0.1 in ethanol and observed no effect of the light intensity on this yield. Molecular oxygen had no effect on the reaction yield. In the presence of a triplet sensitizer the N-oxide $BPQO_2$ undergoes a different photoreaction with a lower yield. This suggests that the photoreaction of $BPQO_2$ is mono-photonic and occurs via excited singlet states. Masoud and Olmsted [4] and earlier Haddadin and Issidorides [3] proposed a mechanism for the reaction via a sequence of oxaziridine formations and migrations of moieties. Yet, since the authors mostly relied on steady state data, this mechanism is not supported by experimental data. As first steps towards a mechanistic understanding of this and related reactions we will here report on its kinetics. It will be shown that the reaction involves processes with time constants ranging from below picoseconds to minutes. Steady state, femtosecond, and nanosecond absorption spectroscopy will give an overview of the kinetics. Fluorescence techniques will allow to identify processes involving excited singlet states. Time-resolved IR spectroscopy will add information on kinetic channels competing with the product formation. For the sake of comparison with the results of Masoud and Olmsted [4] most experiments have been performed in ethanolic solution.

* Corresponding author. Tel.: +49 89 2180 9243; fax: +49 89 2180 9202.
E-mail address: Peter.Gilch@physik.lmu.de (P. Gilch).

1010-6030/$ – see front matter © 2009 Elsevier B.V. All rights reserved.
doi:10.1016/j.jphotochem.2009.05.015

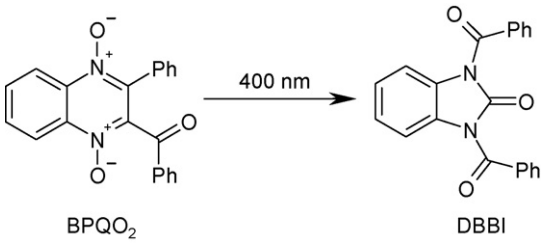

Scheme 1.

2. Materials and methods

The instruments for time-resolved spectroscopy used in the study will be characterized in the same order as the respective measurements are presented in Section 3. The set-up for femtosecond transient absorption measurements has been described in Ref. [5]. In the experiments described here the sample was excited with femtosecond laser pulses. The pump pulses had a center wavelength of 402 nm, an energy of 300 nJ and the repetition rate of the experiment was 1 kHz. At the sample location the pump beam had a diameter of 120 μm. Absorption changes were probed by a white light continuum generated in CaF_2. At the sample the diameter of the white light beam was 50 μm. The relative orientation of the polarization vectors of pump and probe light was set to magic angle. After the sample the white light was dispersed and its spectrally resolved intensity was recorded by a diode array. The time resolution of the experiment was 100 fs (FWHM of the instrumental response function). Sample solutions (typical total volume of 50 ml, concentrations of ~1 mM) were pumped through a fused silica flow cell (pathlength 0.5 mm) placed at the focal point of the two laser beams. For the data presented, at every setting of the delay line the signal of 1000 laser shots was accumulated and the result of 15 scans of the delay line was averaged.

The nanosecond absorption measurements were performed in the lab of Thomas Kiefer (TU München). The set-up has been described in detail elsewhere [6]. Briefly, a pulsed Nd:YAG laser (354.6 nm, 4-ns pulse of 50 mJ; Quantel, Santa Clara, CA) was used to excite the N-oxide sample in a 1 cm fused silica cuvette. The sample concentration was adjusted to ~50–100 μM and the solution was stirred during the experiments. The absorbance changes in the sample after a single laser shot, at certain detection wavelengths, were recorded using a Laser Flash Photolysis Reaction Analyzer (LKS.60; Applied Photophysics, Leatherhead, UK) in combination with a grating monochromator.

The Kerr gate set-up for the femtosecond fluorescence experiments has been detailed in Ref. [7]. It was slightly modified to decrease the intensity of fluorescence light leaking through the closed Kerr gate. The modifications will be described in a forthcoming publication. The sample solution was excited at 387 nm by femtosecond pump pulses. The energy of the pump pulse was 850 nJ and the diameter of the pump beam at the sample 150 μm (repetition rate of 1 kHz). The fluorescence emission was detected in a backscattering geometry, guided through the Kerr gate and detected after spectral dispersion with a CCD camera. The time resolution of the experiment was 200 fs (FWHM of the instrumental response function). The angle between the polarization vector of the pump beam and the transmission axis of the first polarizer of the Kerr gate was 45°. Sample solutions (typical total volume of 10 ml, concentrations of 1 mM) were pumped through a fused silica flow cell (pathlength 1 mm) placed at the focal point of the pump beam. For the data presented here at each setting of the delay the fluorescence signal was accumulated for 10 s and the results of 11 scans of the delay line were averaged.

A description of the instrument for femtosecond IR spectroscopy is given in Refs. [8,9]. A femtosecond laser pulse at 404 nm excited the sample solution (pulse energy 1 μJ, diameter at the sample 150 μm). The induced absorption changes in the mid IR were probed by femtosecond IR pulses (pulse energy ~50 nJ, diameter at the sample 85 μm). After the sample the IR radiation was dispersed and detected with an MCT array. The relative orientation of the polarization vectors of pump and probe light was set to magic angle. Sample solutions (total volume of 50 ml, concentrations of 2.2 mM) were pumped through a home-built flow cell with CaF_2 windows (pathlength 0.22 mm) placed at the focal point of the two laser beams. For the data presented, at every setting of the delay line the signal of 2000 laser shots was accumulated and the result of three scans of the delay line was averaged.

Stationary spectra were recorded with an absorption spectrometer from PerkinElmer (Lambda 19), the fluorescence Kerr gate set-up described above, and an FTIR spectrometer (IFS 66 from Bruker). For continuous wave illumination a mercury xenon lamp (LC4 from Hamamatsu) was used. Long pass filters were used to suppress the UV light so that most of the excitation light was centered around ~400 nm. The spectrally integrated power of the excitation light was ~30 mW.

$BPQO_2$ was synthesized according to Ref. [10], purified by repeated recrystallisation from methanol, and characterized by NMR and IR spectroscopy. All solvents were of spectroscopic grade.

All emission data presented have been corrected for the spectral sensitivity of the instruments. The spectral dependence of time zero in the femtosecond data due to group velocity dispersion has been taken in account. The global fitting routine yielding time constants τ_i and amplitude spectra A_i is specified in Refs. [11–13]. Briefly, a two-dimensional data set $I(\lambda, t)$ is recorded, λ is the detection wavelength (in the IR experiment it is replaced by the detection wavenumber $\tilde{\nu}$), and t is the delay time between excitation and probing. The signal $I(\lambda, t)$ is modelled by the following trial function

$$I(\lambda, t) = \mathrm{IRF} \otimes \sum_{i=1}^{n} A_i(\lambda) e^{-t/\tau_i} \quad t \leq 0. \tag{1}$$

IRF⊗ stands for the convolution with the instrumental response function. The IRF is taken to be a Gaussian with FWHM values given above. The number n of the exponential terms considered is adapted for each experiment.

3. Results

3.1. Absorption spectroscopy

The absorption spectrum of $BPQO_2$ dissolved in ethanol (Fig. 1) exhibits a lowest energy transition peaking at 393 nm (ϵ_{393} =12,200 $M^{-1}\,cm^{-1}$). The spectrometric values are in agreement with earlier evaluations [4]. In cyclohexane the absorption band peaks at 416 nm. This hypsochromic shift with decreasing polarity matches the reported negative solvatochromism of N-oxides (see e.g. [14]). Continuous wave irradiation of a ethanolic solution with ~400 nm light results in a decrease in absorbance around 390 nm and a slight increase around 320 nm. In the early stages of the illumination isosbestic points at 350 nm and 300 nm are observed (Fig. 1a). For that period and suitable concentrations a plot of the absorbance versus time is linear. The slope of this plot affords the quantum yield ϕ_p of the reaction. The value determined here is 0.089 and is close to the value of 0.099 reported earlier [4]. For longer illumination periods the isosbestic points vanish. This behavior can be ascribed to a slow thermal reaction: when a solution of $BPQO_2$ is illuminated for a few minutes and then left in the dark spectroscopic changes are observed which result in a loss of the isosbestic points (Fig. 1a). These changes obey clean first order

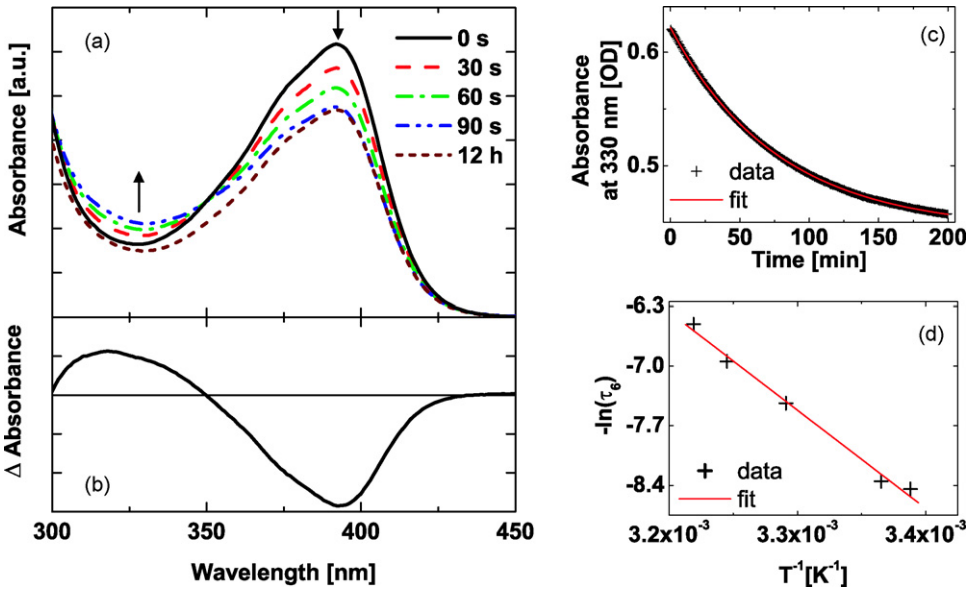

Fig. 1. Changes of the absorption spectrum of $BPQO_2$ induced by cw illumination at 400 nm. (a) Spectra of $BPQO_2$ in ethanol before illumination and after consecutive illuminations for times indicated. The absorbance around 400 nm decreases with illumination. Isosbestic point at 350 nm and 300 nm are seen. Leaving an illuminated sample in the dark results in further spectral changes as the spectrum after 12 h shows. The isosbestic difference spectrum (defined in the text) is given in (b). (c) Temporal evolution of the absorbance at 330 nm of an illuminated sample left in the dark ($T = 295$ K). The crosses are experimental values, the line represents the result of an exponential fit. (d) Arrhenius plot for the dark reaction.

kinetics with a time constant τ_6 of 77 min at 295 K (Fig. 1c). The Arrhenius plot for this time constant is linear in the temperature range from 295 K to 311 K (Fig. 1d). Its slope yields an activation energy of 7600 cm^{-1}. The time constant of this dark reaction is of the same magnitude as the illumination periods of ~10 min commonly used. Therefore, one observes a deviation from isosbestic behavior in an ordinary illumination experiment. For the below treatment of the transient absorption data a difference spectrum is required which characterizes the spectroscopic signatures towards which the transient data converge. Usually, such a difference spectrum is given by the spectrum of the (final) photoproduct minus the spectrum of the starting material. In the present context, it is appropriate to use a difference spectrum computed from those spectra which exhibit isosbestic points. We will refer to this spectrum (Fig. 1b) as the isosbestic difference spectrum and stress that this is not the DBBI minus $BPQO_2$ spectrum.

The following transient absorption experiments will reveal the complex kinetics which finally build up the isosbestic difference signature. In the femtosecond measurements the pump pulse at 402 nm was in resonance with the lowest absorption band of $BPQO_2$. Changes of the absorption induced by this excitation were probed by a white light continuum (Fig. 2). Around time zero the transient absorption spectrum has a negative contribution (absorption bleach) at around 390 nm. The bleach indicates transfer of population from the $BPQO_2$ ground state to a singlet excited state. Deviations of the bleach spectrum from the spectrum of $BPQO_2$ are due to excited state absorption (ESA) spectrally overlapping with the bleach. For wavelengths larger than 400 nm ESA dominates and only positive signals are observed. The positive signal is characterized by a dip around 450 nm and a shallow peak at 600 nm. The dip could result from stimulated emission "cutting into" the ESA. In the spectrum recorded 10 ps after excitation neither the dip nor the peak are present. Apart from the bleach the difference spectrum is now characterized by a positive contribution monotonically decreasing with increasing wavelength. At even later delay times the spectrum further changes in shape and amplitude approaching an offset spectrum for the largest delay time of 1.5 ns covered in the femtosecond experiment. Quantitative kinetic data was retrieved from the femtosecond data using a global multi-exponential fitting procedure. Inspection of representative time traces (two are shown in Fig. 2) indicates that at least three exponential terms and an offset are required to describe the data. The resulting time constants are $\tau_2 = 0.6$ ps, $\tau_3 = 7$ ps, and $\tau_4 = 200$ ps. The errors of these time constants are around 30%. These values are compiled in Table 1. The spectrum recorded after 1.5 ns does not match the isosbestic difference spectrum (Fig. 3a). The latter only features positive difference signatures for wavelengths smaller than 350 nm whereas the 1.5 ns spectrum is positive except for a region around 400 nm. Obviously spectroscopic changes have to happen after 1.5 ns.

These changes were probed using nanosecond laser flash photolysis. One set of experiments was performed with air saturated solutions. For the detection tuned to 390 nm — close to the absorption maximum of $BPQO_2$ — one observes an initial bleach which partially recovers. The initial amplitude of the bleach and the

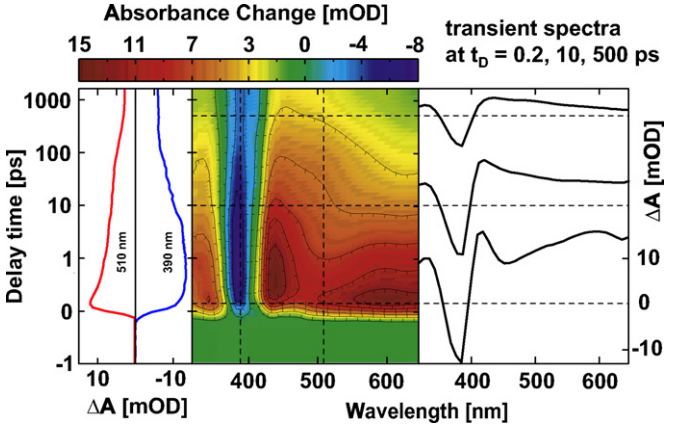

Fig. 2. Absorption changes induced by femtosecond excitation of a $BPQO_2$ solution at 402 nm. In the central contour representation red (blue) coloring stands for a positive (negative) transient absorption. Difference spectra are given on the right, the dashed horizontal lines relate them with the contour plot. The dashed vertical lines mark the spectral positions for the time traces on the left. The time axis is linear from −1 ps to 1 ps and logarithmic thereafter. (For interpretation of the references to color in this figure legend, the reader is referred to the web version of the article.)

Table 1
Time constants of the $BPQO_2$ reaction determined by different time-resolved techniques. For the transient absorption data the "+" sign marks processes which involve ground recovery. For the IR data the relative amplitude of the recovery is given. "n.o." stands for not observed, "n.m." for not measured. The relative errors of the time constants are around ±30%.

Time constant	Absorption	Ground state recovery	Fluorescence	IR	Relative amplitude
τ_1	n.o.	n.o.	0.2 ps	n.o.	n.o.
τ_2	0.6 ps	–	1 ps	0.8 ps	0.25
τ_3	7 ps	+	11 ps	12 ps	0.4
τ_4	200 ps	+	170 ps	160 ps	0.15
τ_5	8 μs	+	n.o.	n.m.	n.m.
τ_6	77 min	–	n.o.	n.m.	n.m.

plateau onto which it decays were used for the relative scaling of the spectra in Fig. 3a. The relative magnitude of the 1.5 ns spectrum was given by the initial amplitude of the 390 nm time trace and the relative magnitude of the isosbestic difference spectrum by the height of the plateau. Based on this scaling predictions are possible how the signal should change on the nano- to microsecond time scale. At 320 nm a positive signal should decrease towards positive pedestal, at 420 nm an initially positive signal should turn negative, and at 470 nm a positive signal should decay to zero. All that is observed in Fig. 3b. The time constant $\tau_5^{O_2}$ with which the signal converges to the isosbestic difference signature is ~250 ns. The lifetime τ_5 proves to be highly sensitive to the oxygen concentration. Degassing the solution by freeze–thaw cycles increases the lifetime τ_5 from 250 ns to 8 μs (Fig. 3c). This strongly suggests that the spectroscopic species observed in this time window has triplet multiplicity.

3.2. Fluorescence spectroscopy

Time-resolved fluorescence spectroscopy can identify kinetic processes involving excited singlet states. Therefore, the transient absorption data are here supplemented by fluorescence results. Upon 388 nm excitation $BPQO_2$ dissolved in ethanol emits a weak fluorescence peaking at 560 nm (Fig. 4). The Stokes shift amounts to 7600 cm^{-1}, in cyclohexane (4200 cm^{-1}) it is considerably smaller. In addition to the peak at 560 nm a shoulder at 450 nm is discernible. The fluorescence quantum yield ϕ_f was determined by comparison of the spectrally integrated fluorescence emission of $BPQO_2$ with that of coumarin 153. Based on the reported yield $\phi_f(\text{coumarin}) = 0.38$ of coumarin 153 [15] a value of $\phi_f(BPQO_2) = 7 \times 10^{-4}$ is obtained. Using this value and the radiative lifetime τ_0 an averaged fluorescence lifetime $\langle\tau_{fl}\rangle$ can be estimated.

$$\langle\tau_{fl}\rangle = \phi_{fl}\tau_0 \quad (2)$$

The Strickler–Berg relation [16] yields a radiative lifetime τ_0 of ~10 ns which translates into an averaged fluorescence lifetime $\langle\tau_{fl}\rangle$ of 7 ps. It is stressed that this is an averaged lifetime and it will be now shown that the fluorescence decay is in fact multi-exponential. The fluorescence decay was traced using the Kerr gate set-up. A solution of $BPQO_2$ was excited at 387 nm using femtosecond laser pulses. The detection window for the fluorescence emission covered the range of 400–750 nm (Fig. 5). Initially, the fluorescence peaks at the blue edge of our detection window. Within well below one picosecond the spectrum changes in shape and amplitude and peaks at 500 nm after 0.6 ps. The fluorescence signal further decays and redshifts on the 1–100 ps time scale. As in the transient absorption experiments time constants were retrieved using the global analysis specified above. Inspection of time traces in the blue, central, and red part of the detection window shows that at least four exponential terms are required (see Fig. 5). The fit affords time constants of $\tau_1 = 0.2$ ps, $\tau_2 = 1.0$ ps, $\tau_3 = 11$ ps, and $\tau_4 = 170$ ps. The constants τ_2– τ_4 are close to the values obtained by transient absorption spectroscopy (see Table 1). The shortest time constant τ_1 is only observed in the fluorescence experiment. Additional information on the spectral distribution of the time constants is given by the decay associated spectra $A_i(\lambda)$ (Fig. 6) which also result from the global fit. Each spectrum $A_i(\lambda)$ represents the spectroscopic changes caused by the kinetic process with the time constant τ_i. The four decay associated spectra show the trend that for larger detection wavelengths longer decay times are observed. The spectrum $A_1(\lambda)$ has its largest values at the blue edge of the detection window and is by roughly an order of magnitude higher in intensity as compared to the other three spectra. For detection wavelengths larger than 490 nm the spectrum is negative. Since a fluorescence signal can only be positive this negative signal represents a delayed rise. In other words, the rapid fluorescence decay in the blue part of the spectrum goes along with a rise in the red part. The spectrum $A_2(\lambda)$ peaks at 470 nm and is positive throughout. Its amplitude is comparable with that of the spectrum $A_3(\lambda)$ which peaks at even longer wavelengths (510 nm) and is also positive throughout. The slowest fluorescence contribution (time constant τ_4 of 170 ps) is associated with a spectrum peaking at 545 nm. The peak of the spectrum $A_4(\lambda)$ has about half the value of that of $A_3(\lambda)$. The temporal integral of the time resolved fluorescence data matches the steady state fluorescence spectrum. This gives confidence that no components longer lived than τ_4 contribute to the steady state fluorescence.

3.3. IR spectroscopy

The photochemical yield ϕ_p of $BPQO_2$ is ~0.1. Thus, photophysical processes recovering the starting material compete with the photochemical pathway. Information on this kinetic competition is obtained by measuring the recovery of the $BPQO_2$ ground state. In the UV/vis transient absorption experiments described above a bleach recovery was recorded from which such information could be retrieved. However, in the spectral range of the absorption of $BPQO_2$ positive transient absorption contributions are superimposed onto the ground state bleach (see above). This obstructs a quantitative analysis. The IR spectrum of $BPQO_2$ offers distinct bands which allow to measure the amount of ground state recovery. Two IR bands of $BPQO_2$ are particularly suited (Fig. 7): the intense band at 1340 cm^{-1} which can be assigned to a N–O stretch mode of the N-oxide [17,18] and the carbonylic stretch mode of the benzoyl moiety at 1690 cm^{-1} [19]. In a steady state illumination experiment an isobestic difference spectrum was recorded (Fig. 7b). Due to the illumination the band at 1340 cm^{-1} experiences a pronounced bleach. A weaker bleach is seen at the spectral position of the benzoylic carbonyl mode at 1690 cm^{-1}. New bands are seen to grow in the high frequency part of the carbonyl range.

In a femtosecond IR experiment a solution of $BPQO_2$ was excited by 404 nm femtosecond laser pulses (Fig. 8). The induced changes in the IR absorption were probed in the N–O stretch and the carbonyl range. The kinetic data retrieved from either range are similar and so the description here is confined to the carbonyl range. Around time zero pronounced bleaches at 1690 cm^{-1} and 1600 cm^{-1} are observed. A weak positive transient IR signal is superimposed. The

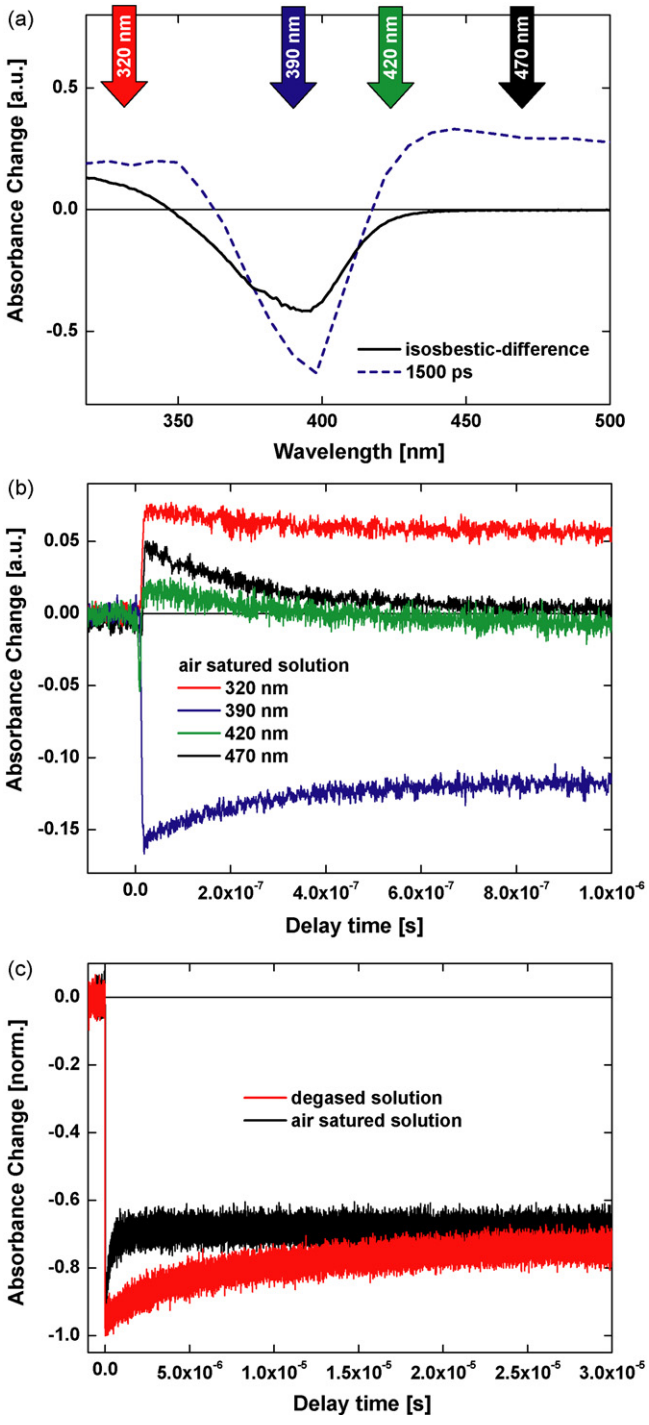

Fig. 3. Nanosecond laser flash photolysis data on the $BPQO_2$ reaction. The excitation wavelength was 355 nm. (a) Difference absorption spectrum after 1.5 ns (taken from the data depicted in Fig. 2) in comparison with the isosbestic difference spectrum. (b) Flash photolysis time traces for detection wavelengths marked in (a). Sample solution was saturated with air. (c) Time traces at 390 nm for air saturated (black) and degassed (red) solutions. (For interpretation of the references to color in this figure legend, the reader is referred to the web version of the article.)

positive signal is spectrally broad and covers the whole detection range. It decays with less than 1 ps. Two positive bands at ~1590 cm^{-1} are longer lived and decay within ~10 ps. The only positive signature observed after 1 ns is a band around 1675 cm^{-1} adjacent to the benzoylic bleach. From the temporal evolution of this bleach information on the ground state recovery can be gained.

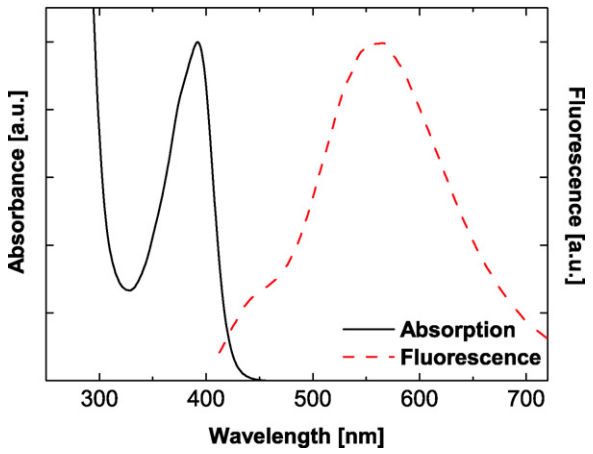

Fig. 4. Absorption and fluorescence emission spectrum of $BPQO_2$ dissolved in ethanol. In the fluorescence experiment the excitation was tuned to 388 nm.

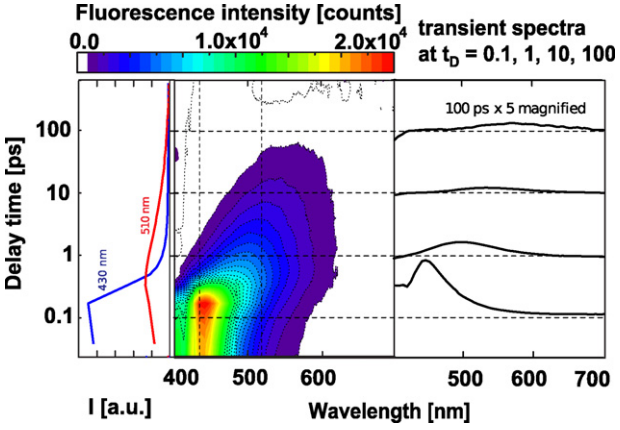

Fig. 5. Femtosecond fluorescence data on the $BPQO_2$ reaction. The ethanolic sample solution was excited with 388 nm femtosecond pulses and the resulting emission was time-resolved using a Kerr gate. In the central contour representation red coloring stands large fluorescence signals. Transient spectra are given on the right, the dashed horizontal lines relate them with the contour plot. The dashed vertical lines mark the spectral positions for the time traces on the left. Note the logarithmic time axis. (For interpretation of the references to color in this figure legend, the reader is referred to the web version of the article.)

A global fit of the IR data yields time constants which agree well with the other experiments (see Table 1). The benzoylic bleach recovers with the time constants (approximate relative amplitudes in brackets) $\tau_2 = 0.8$ ps (0.25) $\tau_3 = 12$ ps (0.4) and $\tau_4 = 160$ ps (0.15). We note that the τ_2 process does not carry ground state recovery amplitude in the visible experiment. The residual bleach after 1 ns relative to the bleach at time zero amounts to ~0.2.

4. Discussion

The kinetic measurements on the light-induced rearrangement of $BPQO_2$ to DBBI yielded time constants covering 16 orders of magnitude. The determination of the shortest time constant $\tau_1 = 0.2$ ps has required a femtosecond fluorescence set-up. The longest time constant $\tau_6 = 77$ min has been determined using a conventional absorption spectrometer.

In the following we will attempt to assign these time constants. The fluorescence data show that the time constants τ_1–τ_4 are associated with singlet excited states. Since $BPQO_2$ exhibits a pronounced (negative) solvatochromism it is expected that the fluorescence dynamics is partially due to dynamic solvation [20]. Dynamic solvation is a multi-exponential process with characteristic times in the range of ~0.1–30 ps for solvents like ethanol [21,22].

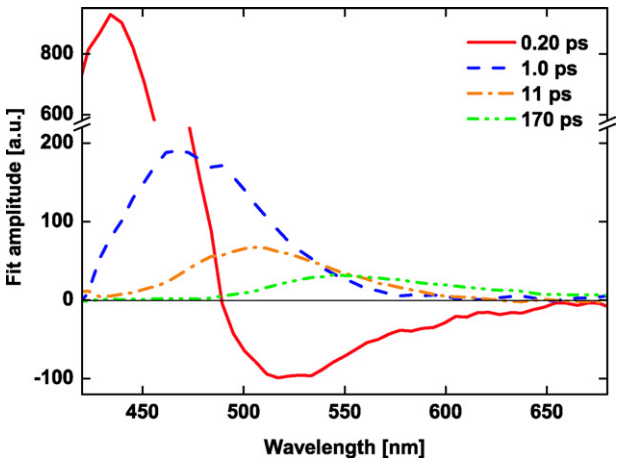

Fig. 6. Decay associated spectra obtained from a global analysis of the femtosecond fluorescence data given in Fig. 5.

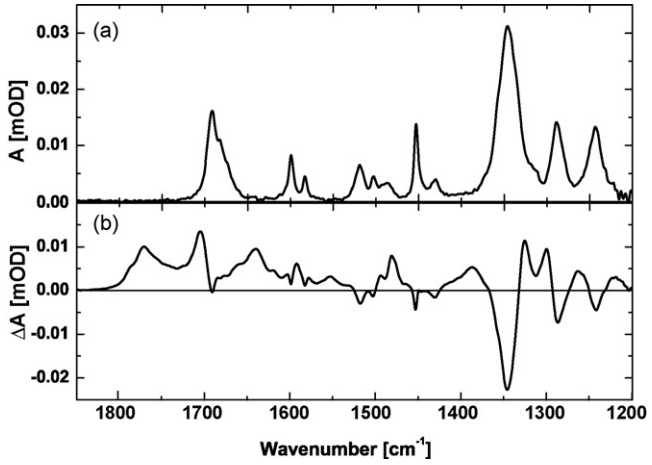

Fig. 7. IR spectrum of $BPQO_2$ (solvent subtracted (a)) and isosbestic difference spectrum (b). For reasons of transmission around 1300 cm^{-1} the spectra were recorded with perdeuterated methanol as a solvent. To record the difference spectrum the sample solution was illuminated for 30 s and the spectra after and before illumination were subtracted.

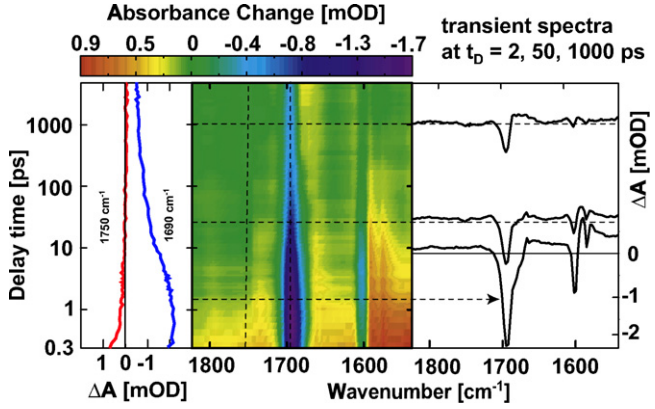

Fig. 8. IR absorption changes induced by femtosecond excitation of a $BPQO_2$ solution (solvent ethanol-d1) at 404 nm. In the central contour representation red (blue) coloring stands for a positive (negative) IR difference absorption. Difference spectra are given on the right, the dashed horizontal lines relate them with the contour plot. The dashed vertical lines mark the spectral positions for the time traces on the left. The time axis is linear from 0.3 ps to 1 ps and logarithmic thereafter. (For interpretation of the references to color in this figure legend, the reader is referred to the web version of the article.)

It results in a red-shift of the fluorescence emission. Inspection of the decay associated spectra in Fig. 6 shows that after each decay component the fluorescence peaks at longer wavelengths. Based on the similarities with the values in Ref. [21] processes with the time constants τ_1– τ_3 could be assigned to dynamic solvation. (It should be noted that in studies on dynamic solvation one commonly relies on the time evolution of a spectral response function [21,22]. Such a treatment differs from the one employed here and therefore allowance should be made for difference between the time constants τ_1– τ_3 determined here and those in solvation studies.) It is well possible that the intermolecular process of dynamic solvation is accompanied by intramolecular changes of the photo-excited $BPQO_2$. The τ_1– τ_3 processes not only shift the fluorescence emission to the red but also reduce the spectrally integrated emission. For "pure" solvation processes this integrated signal is expected to remain constant [21]. Structural distortions of the excited $BPQO_2$ could — via a non-Condon effect — reduce the spectrally integrated fluorescence emission during that stage (for a recent description see e.g. [23]). For the τ_1 process this seems to be the most likely explanation. Excited state depletion contributes to the decay of the spectrally integrated fluorescence signal for the components with time constants τ_2– τ_4. This can be inferred from the IR and the UV/vis experiments which agree that a recovery occurs with the constants τ_3 and τ_4. A recovery characterized by τ_2 was only detected in the IR experiment.

The time constants τ_2, τ_3. and τ_4 can thus be considered as "lifetimes" of excited singlet states. The values of $\tau_2 \approx 1$ ps and $\tau_2 \approx$ 10 ps are of the same magnitude as the time constant of 3.1 ps reported for quinoxaline-di-N-oxide (QO_2) [24], the parent compound of $BPQO_2$. In the study on QO_2 a single exponential decay of the excited state was observed. The multi-exponential decay reported here for $BPQO_2$ can in principle be attributed to various effects. (i) *Ground state heterogeneity.* In thermal equilibrium different conformers of $BPQO_2$ might coexist which could differ in their excited state behavior. Inspection of the X-ray structure of $BPQO_2$ [25] shows that each of its three ring systems is essentially planar. The main structural variants are thus only the torsional angles of the phenyl- and the benzoyl-substituents with respect to the quinoxaline-di-N-oxide system. In the crystalline state these angles are 70° for the phenyl moiety and 103° for the benzoyl residue. (Note that the two conformers described in Ref. [25] are enantiomers.) Steric constraints are expected to exclude larger deviations from this pronounced non-coplanarity also in solution phase. This renders a ground state heterogeneity as cause for the multiphasic emission decay unlikely. (ii) *Sequential kinetics in the excited state.* From the Franck Condon region of the excited singlet state of $BPQO_2$ a minimum on its potential energy surface must be accessible. Otherwise no longer lived fluorescence components should be detectable. The population in the minimum might then be partially transferred to other electronic states and partially to a second minimum of the excited state and so on. For sequential kinetics one should expect a τ_3 rise components in the fluorescence data, i.e. a negative contributions in the decay associated spectra. Since such contributions are absent (Fig. 6) — except for the τ_1 process — one is tempted to rule out sequential kinetics. Yet, provided that the oscillator strength for the second minimum is smaller than the one for the first minimum and their fluorescence spectra overlap such a rise need not show up. (iii) *Branched kinetics in the excited state.* Alternatively, the three minima might be populated simultaneously during an early branching which would occur during the τ_1 process. After that branching the minima would be kinetically separated. The spectroscopic data are in line with this branched scenario. Based on the present findings it is considered the most probable one.

What applies to all scenarios is that after the τ_4 process the fraction f_{nr} of $BPQO_2$ not recovered is 0.2. It is larger than the pho-

tochemical yield ϕ_p of ~0.1 determined by Masoud and Olmsted [4] and in this study. The fraction f_{nr} represents those molecules which are in a precursor state for the final photoproduct and in other longer lived states. To some part the triplet yield ϕ_t contributes to f_{nr}. The transient absorption spectrum recorded after the τ_4 process has a very broad positive contribution extending from ~400 nm to 600 nm. Such spectral features have been ascribed to triplet states of other aza-anthracene-N-oxides [26,27]. Further, in the nanosecond experiment (Fig. 3) a decay time $\tau_5^{O_2}$ of 250 ns has been observed for $BPQO_2$ in air saturated ethanol. This decay time is in the typical range for diffusion controlled triplet quenching by molecular oxygen [28]. Accordingly, degassing prolongs the τ_5 time constant. The τ_5 process can thus unequivocally be assigned to the decay of the triplet state of $BPQO_2$. An upper boundary for the triplet yield ϕ_t of $BPQO_2$ is given by $f_{nr} - \phi_p = 0.1$. The triplet state does not contribute to the formation of DBBI. Masoud and Olmsted [4] have shown that the product yield ϕ_p is not sensitive to the oxygen concentration whereas it is shown here that the triplet lifetime is very sensitive. This excludes formation of DBBI via a triplet state. Likewise, flash photolysis experiments on QO_2 show that a triplet state albeit populated does not participate in the formation of a photoproduct [26].

In our nanosecond data all spectroscopic changes are attributable to the decay of the triplet state. Yet, inspection of the IR difference spectra (Figs. 7 and 8) point to additional kinetics in the nanoseconds to seconds time window. The IR difference spectrum recorded after 1 ns lacks a positive absorption band at 1750 cm^{-1} which is very pronounced in the isosbestic difference spectrum. This band has to build up in less than ~1 s. We have not performed time-resolved IR spectroscopy in this time window and the process does not leave an imprint in nanosecond data recorded in the visible range. So at present we cannot be more specific about this process or processes. The authors of the flash photolysis experiment on QO_2 suggested that within their time resolution (~10 μs) an oxaziridine intermediate is formed and that this intermediate transforms into the 2-quinoxaline-4-oxide product within 0.01 s [26]. For $BPQO_2$ this could imply that an oxaziridine intermediate is present after the τ_4 process. It rearranges on multiple time scales to finally yield DBBI. The isosbestic IR difference spectrum suggests that after — say — a few seconds at latest the benzimidazolone framework of DBBI is already present. In the carbonyl range the spectrum features a band at 1750 cm^{-1}. Such a high frequency of a carbonyl mode is characteristic for benzimidazolones [29]. Obviously, an important structural marker of the DBBI photo-product is present prior to the final τ_6 process. This process could involve hindered rotation of the benzoyl moieties with respect to the imidazolone body. The rotation constitutes the well-studied hindered rotation of an amide bond. Typical (free energy) barriers for these rotations are in the range of ~5000–10,000 cm^{-1} [30] in accordance with the present finding. So hindered rotations around amide bonds seem to terminate the photoreaction.

5. Conclusion

Heteroaromatic N-oxides exhibit a very rich and diverse photochemistry. The present study on $BPQO_2$ shows that this richness finds its counterpart in the photokinetics. Photo-excitation of $BPQO_2$ triggers processes with time constants from 200 fs to 77 min (cf. Fig. 9). The earliest of these processes can be ascribed to dielectric relaxation of the solvent. Photochemistry "starts" with the depletion of the excited singlet manifold which is multi-phasic with time constants of ~1 to ~200 ps. In the course of this depletion a triplet state and a product precursor are formed. The triplet state does not contribute to the photo-reactivity. The final transformation of the precursor(s) to the product takes 77 min and could be related to the isomerization around an amide bond. The broad range of time constants observed translates into large variation of activation barriers. Thereby, $BPQO_2$ seems to be a very good tool to study organic reactivity. This and the structural assignment of the intermediates involved is subject of present studies.

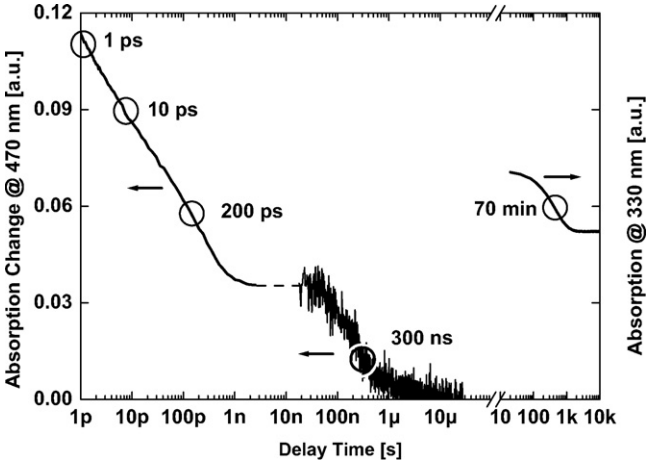

Fig. 9. Overview of the photokinetics of $BPQO_2$ based on femtosecond, nanosecond and cw-absorption data. The graph highlights the huge range of time scales involved. Note that the shortest processes which shows up in the fluorescence experiment is not even included.

Acknowledgments

This work was supported by the Deutsche Forschungsgemeinschaft through the DFG-Cluster of Excellence Munich-Centre for Advanced Photonics and SFB 749 (A5). We thank our undergraduate Axel Beyer for recording some of the cw absorption data. We further thank Fabian Michalik and Karola Rück-Braun (TU Berlin) for experimental support.

References

[1] G.G. Spence, E.C. Taylor, O. Buchardt, Photochemical reactions of azoxy compounds, nitrones, and aromatic amine n-oxides, Chem. Rev. 70 (1970) 231–265.
[2] A. Albini, M. Alpegiani, The photochemistry of the n-oxide function, Chem. Rev. 84 (1984) 43–71.
[3] M.J. Haddadin, C.H. Issidorides, Photolysis of a quinoxaline-di-n-oxide, Tetrahedron Lett. (1967) 753–756.
[4] N.A. Masoud, J. Olmsted, Photochemistry of 2-benzoyl-3-phenylquinoxaline 1,4-dioxide, J. Phys. Chem. 79 (1975) 2214–2220.
[5] T. Cordes, D. Weinrich, S. Kempa, K. Riesselmann, S. Herre, C. Hoppmann, K. Rück-Braun, W. Zinth, Hemithioindigo-based photoswitches as ultrafast light trigger in chromopeptides, Chem. Phys. Lett. 428 (2006) 167–173.
[6] F. Krieger, B. Fierz, O. Bieri, M. Drewello, T. Kiefhaber, Dynamics of unfolded polypeptide chains as model for the earliest steps in protein folding, J. Mol. Biol. 332 (2003) 265–274.
[7] B. Schmidt, S. Laimgruber, W. Zinth, P. Gilch, A broadband Kerr shutter for femtosecond fluorescence spectroscopy, Appl. Phys. B 76 (2003) 809–814.
[8] T. Schrader, A. Sieg, F. Koller, W. Schreier, Q. An, W. Zinth, P. Gilch, Vibrational relaxation following ultrafast internal conversion: comparing ir and raman probing, Chem. Phys. Lett. 392 (2004) 358–364.
[9] T.E. Schrader, W.J. Schreier, T. Cordes, F.O. Koller, G. Babitzki, R. Denschlag, C. Renner, M. Loweneckt, S.L. Dong, L. Moroder, P. Tavan, W. Zinth, Light-triggered beta-hairpin folding and unfolding, Proc. Natl. Acad. Sci. U.S.A. 104 (2007) 15729–15734.
[10] M.J. Haddadin, G. Agopian, C.H. Issidorides, Synthesis and photolysis of some substituted quinoxaline di-n-oxides, J. Org. Chem. 36 (1971) 514–518.
[11] H. Satzger, W. Zinth, Visualization of transient absorption dynamics—towards a qualitative view of complex reaction kinetics, Chem. Phys. 295 (2003) 287–295.
[12] B. Heinz, S. Malkmus, S. Laimgruber, S. Dietrich, C. Schulz, K. Ruck-Braun, M. Braun, W. Zinth, P. Gilch, Comparing a photoinduced pericyclic ring opening and closure: differences in the excited state pathways, J. Am. Chem. Soc. 129 (2007) 8577–8584.
[13] T. Cordes, B. Heinz, N. Regner, C. Hoppmann, T.E. Schrader, W. Summerer, K. Rück-Braun, W. Zinth, Photochemical $Z \rightarrow E$ isomerization of a hemithioindigo/hemistilbene omega-amino acid, ChemPhysChem 8 (2007) 1713–1721.

[14] C. Reichardt, Solvatochromism, thermochromism, piezochromism, halochromism, and chiro-solvatochromism of pyridinium n-phenoxide betaine dyes, Chem. Soc. Rev. 21 (1992) 147–153.
[15] G. Jones, W. Jackson, C.-Y. Choi II, Solvent effects on emission yield and lifetime for coumarin laser dyes. Requirements for a rotatory decay mechanism, J. Phys. Chem. 89 (1985) 294–300.
[16] S. Strickler, R. Berg, Relationship between absorption intensity and fluoresence lifetime of molecules, J. Chem. Phys. 37 (1962) 814–822.
[17] M. Khan, M. Qureshi, Y. Ahmad, Studies on heterocyclics. Part III. The IR spectra of some quinoxaline n-oxides, Pakistan J. Sci. Ind. Res. 15 (1972) 252–253.
[18] K.V. Berezin, Quantum-mechanical calculation of the frequencies of the normal vibrations and intensities of the IR and Raman bands of pyridine n-oxide, Opt. Spectrosc. 94 (2003) 179–184.
[19] B. Schrader (Ed.), Infrared and Raman Spectroscopy, VCH, Weinheim, New York, Basel, Cambridge, Tokyo, 1995.
[20] J. Lakowicz, Principles of Fluorescence Spectroscopy, third edition, Springer, New York, 2006.
[21] M.L. Horng, J.A. Gardecki, A. Papazyan, M. Maroncelli, Subpicosecond measurements of polar solvation dynamics: coumarin 153 revisited, J. Phys. Chem. 99 (1995) 17311–17337.
[22] M. Glasbeek, H. Zhang, Femtosecond studies of solvation and intramolecular configurational dynamics of fluorophores in liquid solution, Chem. Rev. 104 (2004) 1929–1954.
[23] K. Ishii, S. Takeuchi, T. Tahara, Pronounced non-condon effect as the origin of the quantum beat observed in the time-resolved absorption signal from excited-state cis-stilbene, J. Phys. Chem. A 112 (2008) 2219–2227.
[24] X. Shi, J. Poole, J. Emenike, G. Burdzinski, M. Platz, Time-resolved spectroscopy of the excited singlet states of tirapazamine and desoxytirapazamine, J. Phys. Chem. A 109 (2005) 1491–1496.
[25] Y. Wang, H.Q. Wang, Q.G. Wang, Structure of 3-benzoyl-2-phenylquinoxaline 1,4-dioxide, Acta Crystallogr. Sect. C: Crystal Struct. Commun. 47 (1991) 845–848.
[26] H. Kawata, K. Kikuchi, H. Kokubun, Studies of the photoreactions of heterocyclic n-dioxides—identification of the oxaziridine intermediate of quinoxaline-1,4-dioxide, J. Photochem. 21 (1983) 343–350.
[27] X. Shi, M. Platz, Time resolved spectroscopy of some aromatic N-oxide triplets, radical anions, and related radicals, J. Phys. Chem. A 108 (2004) 4385–4390.
[28] N. Turro, Modern Molecular Photochemistry, The Benjamin/Cummings Publishing Co. Inc., Menlo Park, CA, 1978.
[29] Y.A. Rozin, E.P. Darienko, Z.V. Pushkareva, Synthesis and properties of aroyl derivatives of 2-imidazolone and 2-benzimidazolone, Chem. Heterocycl. Compds. 4 (1971) 510–513.
[30] W.E. Stewart, T.H. Siddall, Nuclear magnetic resonance studies of amides, Chem. Rev. 70 (1970) 517–551.